Metal-insulator transitions and magnetism in correlated band insulators: FeSi and $Fe_{1-x}Co_xSi$

V. V. Mazurenko,[1] A. O. Shorikov,[1,2] A. V. Lukoyanov,[1,2] K. Kharlov,[1] E. Gorelov,[3]
A. I. Lichtenstein,[4] and V. I. Anisimov[1,2]

[1]*Theoretical Physics and Applied Mathematics Department, Urals State Technical University, Mira Street 19, 620002 Ekaterinburg, Russia*

[2]*Institute of Metal Physics, Russian Academy of Sciences, 620219 Ekaterinburg GSP-170, Russia*

[3]*Institut für Festkörperforschung and Institute for Advanced Simulation, Forschungzentrum Jülich, 52425 Jülich, Germany*

[4]*Institute of Theoretical Physics, University of Hamburg, Jungiusstrasse 9, 20355 Hamburg, Germany*

(Received 22 May 2009; revised manuscript received 9 March 2010; published 30 March 2010)

The LDA+DMFT (local density approximation combined with dynamical mean-field theory) computation scheme has been used to study spectral and magnetic properties of FeSi and $Fe_{1-x}Co_xSi$. Having compared different models, we conclude that a correlated band insulator scenario in contrast to Kondo insulator model agrees well with FeSi band structure and experimental data. Coulomb correlation effects lead to band narrowing of the states near the Fermi level with mass renormalization parameter $m^* \approx 2$ in agreement with the results of angle-resolved photoemission spectroscopy. Temperature dependence of spectral functions and magnetic susceptibility calculated in DMFT reproduces transition from nonmagnetic semiconductor to metal with local magnetic moments observed experimentally. Cobalt doping leads to ferromagnetism that has itinerant nature and can be successfully described by the LDA+DMFT method.

DOI: 10.1103/PhysRevB.81.125131 PACS number(s): 71.27.+a, 71.10.−w

I. INTRODUCTION

The narrow-gap semiconductor FeSi demonstrates an interesting interplay between magnetic and electronic properties. Magnetic susceptibility temperature dependence shows maximum at 500 K and Curie-Weiss behavior at higher temperatures.[1] While intrinsic magnetic susceptibility vanishes below 50 K, FeSi does not show any sign of spin ordering down to the lowest temperatures.[2] Photoemission[3] and optical experiments show an energy gap of about 60 meV at low temperatures that is gradually filled with temperature increase.[4] A resistivity temperature dependence shows transition from a narrow-gap semiconductor to a bad metal.[5] Cobalt doping results in ferromagnetic metal state for $Fe_{1-x}Co_xSi$.[6]

Several models have been suggested to explain the unusual temperature dependence of the FeSi physical properties ranging from spin fluctuations[7] to phenomenological models assuming two narrow d bands in the vicinity of the band gap.[8,9] Such density of states (DOS) models are similar to a Kondo insulator description and due to the striking similarities in the physical properties of these Kondo insulators it was claimed that FeSi is the first Kondo insulator containing no f electrons.[10,11]

Historically, the first FeSi model was proposed by Jaccarino *et al.*[1] To describe the unusual magnetic susceptibility and specific heat, a model DOS with extreme narrow-band peaks around a small energy gap was proposed. Despite the fact that the model fitting results were in good agreement with experimental data for the susceptibility this picture contradicts a band structure calculation[12] where no unphysically narrow bands were obtained.

The next model proposed to describe electronic and magnetic properties of FeSi was the Kondo insulator model.[13] The motivation of applying the Kondo model to explain physical properties of FeSi was that the spin-fluctuation spectra of CeNiSn and FeSi are similar. According to this model, a set of localized atomiclike electron levels interact with a wide itinerant band. The insulating state scaled by a Kondo temperature T_K is the result of a weak hybridization between the localized and itinerant bands. The implementation of the Kondo insulator model to FeSi compound is however questionable since the band structure of FeSi shows a strong hybridization between the Fe $3d$ and Si p states. Also the magnetic interactions in FeSi are essentially ferromagnetic and not antiferromagnetic as it would be expected from a Ruderman-Kittel-Kasuya-Yosida (RKKY) picture. For all these reasons it is desirable to have a microscopic model based on the realistic band structure which can reproduce experimental data.

First-principles band structure calculations performed by Mattheis and Hammann[12] have shown that the energy gap value of 0.1 eV is essentially smaller than the width of the band above the Fermi level (~0.5 eV). Band-structure analysis led the authors to conclusion that hybridization between Fe d and Si p states is very strong. These results do not support the Jaccarino's model as well as the Kondo scenario.

Recently, another model of a correlated band insulator (CBIM) was proposed by Kuneš and Anisimov.[14] Using the dynamical mean-field theory (DMFT) the authors have taken into account local dynamical correlations for a gapped local-density approximation (LDA) spectral function of $FeSb_2$ that experimentally demonstrates a temperature-dependent transition from nonmagnetic semiconductor to metal with local moments similar to FeSi. It was found that in DMFT the energy gap is reduced due to the correlation effects by a factor of 2 in comparison with the LDA value. Within the CBIM picture bands above and below the energy gap are formed by nonlocal bonding and antibonding orbital combinations. The account of the on-site Coulomb interaction leads to a competition between localization and formation of the nonlocal bonds. The DMFT calculations allowed then to

TABLE I. Classification of FeSi models.

Jaccarino's model[a]	$W \ll E_{gap}(W \to 0\ \text{K},\ E_{gap}=1520\ \text{K})$
Kondo insulator model[b]	$W=E_{gap}/2(W=500\ \text{K},\ E_{gap}=1000\ \text{K})$
CBIM (this work)	$W \gg E_{gap}(W=5000\ \text{K},\ E_{gap}=1000\ \text{K})$

[a]Reference 1.
[b]Reference 8.

successfully reproduce temperature dependence of magnetic susceptibility, resistivity, and optical conductivity experimentally measured in $FeSb_2$.

Recent angle-resolved photoemission experiments[15] have revealed a considerable renormalization of the energy bands in FeSi. The authors estimated an effective band mass renormalization $m^*/m \approx 2$. As a consequence, the LDA band gap of 100 meV is renormalized by a factor of 0.5–50 meV in agreement with other experimental data.

We summarize the parameters of the models used to describe FeSi in Table I. The basic difference between Kondo insulator and CBIM models is a ratio between the energy gap value E_{gap} and a width W of the bands around the gap. While the Kondo insulator model requires $W/E_{gap} \ll 1$ to give reasonable results, CBIM uses $W/E_{gap} \gg 1$ in agreement with the FeSi realistic band structure.[12]

This paper is aimed to provide microscopic analysis of hybridization and correlation processes in FeSi. We start from construction of a simple band insulator model that captures the essential hybridization effects between Fe $3d$ and Si $3p$ states in FeSi (Sec. II A). This model demonstrates an energy gap that is five times narrower than the width of bands. In order to investigate correlation effects we define a density of states model based on the LDA calculations for FeSi and solve it using the dynamical mean-field theory (Sec. II B). A strong renormalization of DOS near the Fermi level was found in the DMFT calculations that is in good agreement with a band narrowing observed in the recent angle-resolved photoemission spectroscopy (ARPES) experiments. The temperature increase in the DMFT calculations results in a transition from a nonmagnetic insulator to a bad metal with local moments in agreement with experimental data. Having encouraged by these results, we investigated a doped FeSi model to study the magnetic properties of $Fe_{1-x}Co_xSi$ alloys (Sec. III). We demonstrated that a good agreement between calculated and experimental values for magnetization M as a function of doping x can be achieved using the LDA+DMFT method.

II. FeSi

A. Band effects

The crystal structure of FeSi corresponds to four formula units in the unit cell and its band structure is rather complicated for analysis using a simple model. To provide a better understanding of FeSi band structure near the Fermi level Mattheiss and Hamann[12] have proposed to consider the closely related phase with the symmetry of the rocksalt structure. The latter phase can be obtained from original crystal

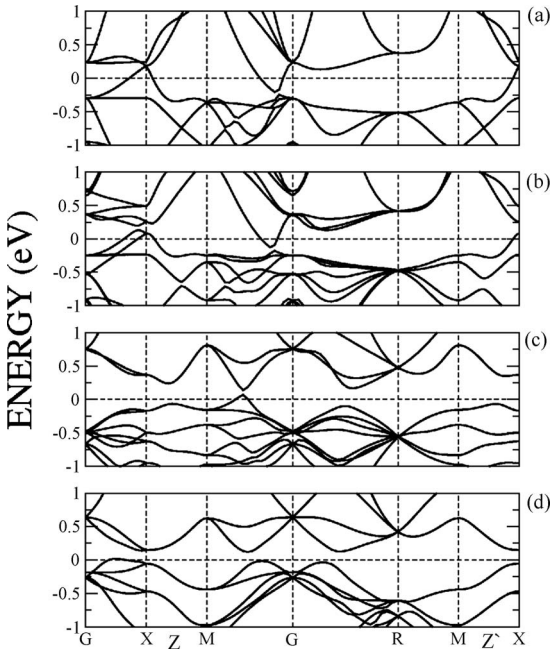

FIG. 1. TB-LMTO energy bands of FeSi obtained with different sets of atomic-position parameters u(Fe) and u(Si). (a) Structure with u(Fe)=0.25 and u(Si)=0.75 corresponds to nonprimitive rocksalt structure that contains four FeSi formula units. Figures (b) and (c) are energy-band results for two transitional structures with u(Fe)=0.23, u(Si)=0.76 and u(Fe)=0.19, and u(Si)=0.79, respectively. Figure (d) corresponds to the real FeSi structure. Symmetry lines are chosen according to Ref. 12.

structure by a relatively small shift of atomic positions. They have shown that the origin of the energy gap in FeSi can be traced to a pseudogap that is already present in the rocksalt phase. This result is a starting point of our investigation that is aimed to construct a minimal realistic band insulator model which captures main features of LDA electronic spectrum of FeSi.

As the first step we studied effects of atomic positions shift on the band picture of FeSi. For that purpose we carried out calculations using the tight-binding linear muffin-tin orbital approach in atomic sphere approximation (STUTTGART LMTO47 code)[16] with conventional LDA. The exchange-correlation potential of the Barth-Hedin-Janak form[17] was used. The crystal structure information about space group, lattice constants, and atomic positions was taken from Ref. 12. The radii of atomic spheres were set to r(Fe) =2.46 a.u. and r(Si)=2.5 a.u.. Two types of empty spheres $r(E_1)=1.62$ a.u. and $r(E_2)=1.13$ a.u. were added. In the orbital basis set the following states were included: Fe($4s$,$4p$,$3d$) and Si($3s$,$3p$). The Brillouin-zone integration has been performed in the grid generated by using (8;8;8) divisions.

Figure 1 gives band structures for real (simple cubic) structure [atomic positions are u(Fe)=0.1358 and u(Si) =0.844], rocksalt (face-centered-cubic)—phase [u(Fe)=0.25 and u(Si)=0.75] and for two model structures with intermediate atomic positions (Fig. 1). The obtained bands agree well with the linear augmented plane-wave (LAPW) results for real and rocksalt phases.[12] The fcc band structure con-

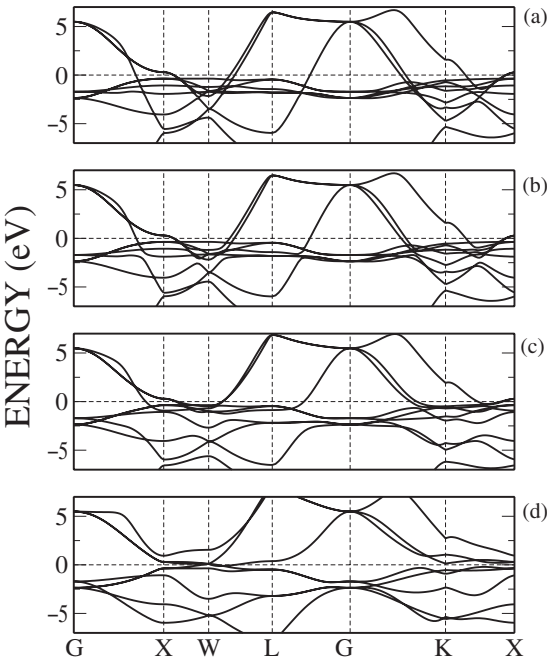

FIG. 2. Band structures for the different degrees of the hybridization strength between Fe 3*d* and Si 3*s*, 3*p* states in fcc crystal structure with one formula unit in unit cell. Figures (a)–(d) are the energy spectra for the hybridization scaling parameter $\alpha=0$, 0.1, 0.5, and 1, respectively. Symmetry lines are chosen according to Ref. 12.

tains several electrons and holes pockets near *G* and *X* points in the Brillouin zone that corresponds to a pseudogap in the energy spectrum in contrast to the real gap in the simple cubic structure. For intermediate structure with atomic-position parameters $u(\mathrm{Fe})=0.19$ and $u(\mathrm{Si})=0.79$, the energy gap is open along all symmetry lines of the Brillouin zone, except the *GM* line. One can see that there is a complete energy gap in the real FeSi structure. This result agrees well with a conclusion of Mattheiss and Hamann[12] that the energy gap state of FeSi results from the distortion of the pseudogapped rocksalt structure.

It is natural to expect that the features of the FeSi electronic spectrum, such as the narrow gap and the peak above the Fermi level, are provided by Fe 3*d* and Si 3*s*, 3*p* states.[12,18] To investigate the origin of the pseudogapped state in the fcc phase we artificially scaled the hybridization strength between Si 3*s*, 3*p*, and Fe 3*d* states. To do so off-diagonal Hamiltonian elements which describe the hybridization between Fe and Si atoms were multiplied by a coefficient $0\leq\alpha\leq1$. These results are presented in Fig. 2.

To simplify our analysis of the band structures, one can consider dispersion curves along *LG* symmetry line where complete energy gap opens due to hybridization between Fe 3*d* and Si 3*s*, 3*p* states. Without hybridization ($\alpha=0$) the wide silicon band crosses three narrow 3*d* bands of iron for *k* vectors along *LG* direction. At increasing hybridization strength [Figs. 2(b) and 2(c)] two of the iron bands strongly interact with silicon states while one of them remains almost unaffected by *d-p* hybridization. The resulting dispersion curves of the fully hybridized system are presented in Fig. 2(d). It means that the pseudogapped state [Fig. 2(d)] originates from a strong hybridization of the wide silicon band ($\approx$10 eV) with the relatively narrow iron band ($\approx$1 eV). The narrow gap opens between antibonding hybridized band above and unhybridized band below the Fermi level.

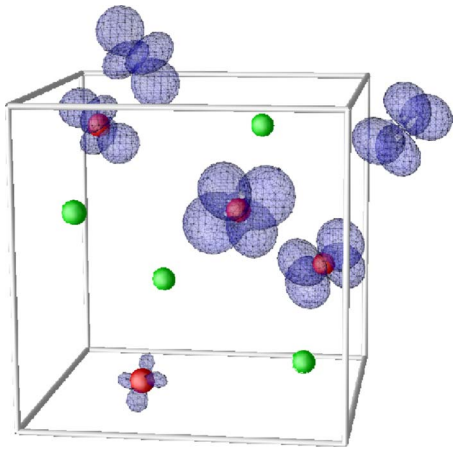

FIG. 3. (Color online) Wannier function corresponding to the first band above the Fermi level [see Fig. 1(d)]. The Wannier function is centered at a 3*d* orbital of iron atom (red spheres). Green spheres correspond to silicon atoms. We found about 40% of the electron density at the central atom and its iron neighbors. The rest of the Wannier function is distributed over many unit cells and is formed by iron and silicon atomic orbitals with contributions of about 1%.

While qualitatively this situation resembles the Kondo insulator picture with weakly hybridized wide and narrow bands, there are two essential quantitative differences. First, the "narrow" band having width of an order of magnitude smaller than the "wide" band is still too wide in absolute value of about 1 eV. Second, *d-p* hybridization is so strong that "pure hybridization" gap in Fig. 2(d) is larger than 2 eV. The small value of the gap is not due to *d-p* hybridization weakness but happens between hybridized and unhybridized bands.

Another argument against the Kondo scenario can be found from analysis of the two bands [Fig. 1(d)] forming a well-separated narrow peak above the Fermi level (Fig. 6). In Kondo system these bands should be associated with strongly localized atomic orbitals of an iron atom. To check this, we calculated the Wannier function for the first conduction band using a projection procedure.[19] A spatial distribution of the calculated Wannier function is shown in Fig. 3. The resulting Wannier function corresponds to a complex combination of 3*d* states of iron and 3*s*, 3*p* states of silicon and is spread over many unit cells. This picture is very far from localized atomic orbital needed for the Kondo scenario and supports the band insulator model.

For *LG* direction we construct an effective microscopic model (Fig. 4) with a minimal set of orbitals that reproduces the gapped state. The model silicon and iron atoms are described with one and two orbitals, respectively. The model Hamiltonian is given by

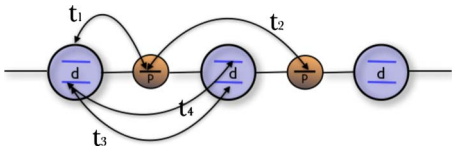

FIG. 4. (Color online) One-dimensional effective model. Large and small circles correspond to iron and silicon atoms in the fcc phase of FeSi.

$$H = \begin{pmatrix} 2t_3\cos(k) & 2t_4\cos(k) & 2t_1\alpha\cos(k/2) \\ 2t_4\cos(k) & 2t_3\cos(k) & 2t_1\alpha\cos(k/2) \\ 2t_1\alpha\cos(k/2) & 2t_1\alpha\cos(k/2) & 2t_2\cos(k) \end{pmatrix},$$

where t_1, t_2, t_3, and t_4 are hoppings between model iron and silicon orbitals presented in Fig. 4, and α is a hybridization scaling parameter. These parameters were calculated for the *LG* model using the real band structure of the full Hamiltonian presented in Fig. 2 as t_1=2.0 eV, t_2=3.0 eV, t_3 =−1.2 eV, and t_4=−0.25 eV. The values are much larger than those calculated for localized systems[20] and are far outside the values range needed for the Kondo insulator scenario.

For the defined above model the band structures with (α=1) and without (α=0) hybridization are presented in Fig. 5. One can see that our model results are in good agreement with those obtained from calculations with full Hamiltonian (Fig. 2). The substantial Fe-Si hybridization leads to splitting into a lower bonding and upper antibonding bands with a nonbonding band in between. We obtained the semiconducting ground state with a small energy gap of 0.8 eV that is much smaller than the narrowest band width of 4.8 eV near the Fermi level. One should note that the small value of the energy gap is not a consequence of a weak Fe-Si hybridization and the minimal realistic band structure model of FeSi

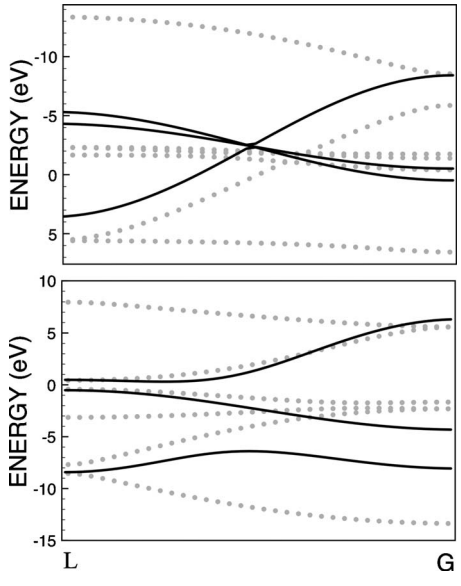

FIG. 5. Model (black solid lines) and real (grey dotted lines) band structures. Lower and upper figures correspond to the models with and without hybridization, respectively.

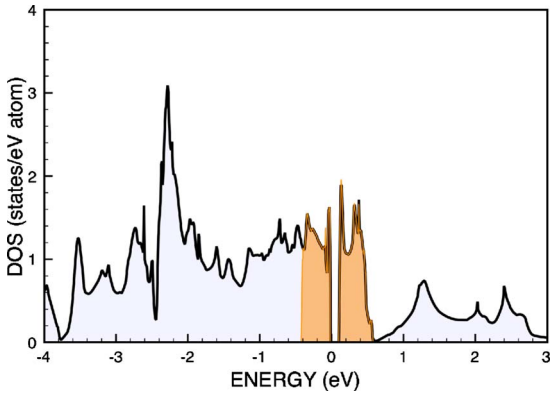

FIG. 6. (Color online) Model (filled area) and full (line) densities of states obtained from LDA calculations.

differs qualitatively from the Kondo insulator regime.

The proposed band model can be used to study Coulomb correlation problem in the framework of static or dynamical mean-field approaches. However, as we will show below, it is possible to define an effective density of states model derived from the full DOS obtained in the LDA calculation for the real crystal structure. Solution of this model by DMFT allows us to describe anomalous physical properties of FeSi.

B. Correlation effects

In this section we study the effects of the Coulomb correlations on the electronic structure and physical properties of FeSi using the dynamical mean-field theory. As an input DMFT requires a noninteracting Hamiltonian or a DOS.[21] The essential features of FeSi density of states obtained in the LDA calculations (Fig. 6) are a small energy gap ≈0.1 eV and a narrow (≈0.5 eV) peak above the Fermi level containing 0.5 electrons per spin per Fe atom. We defined the model density of states (see filled area in Fig. 6) by cutting from the entire DOS area around the Fermi energy with an integral equal to one electron per spin per Fe atom. The model density of states contains the main features of the FeSi spectrum, namely, the energy gap (0.1 eV) and the narrow peak above the Fermi level (0.5 eV).

We would like to stress that a similar density of states model was used in Ref. 27 and 28. To study the correlation effects in FeSi Urasaki and Saso[28] have applied the self-consistent second-order perturbation theory. It was found that the DOS becomes strongly temperature dependent and the peaks of the gap edges move toward the center of the gap. As we will show below the account of the Coulomb correlation effects in the framework of DMFT results in a strong renormalization of the states near the Fermi level.

As impurity solvers of the DMFT problem we used a quantum Monte Carlo method with the Hirsch-Fye algorithm[22] (QMC-HF), a continuous-time quantum Monte Carlo method with interaction expansion[23] (CT-QMC), and an exact diagonalization (ED) temperature-dependent Lanczos[24] approach. Each DMFT techniques was used to describe physical properties of FeSi at different temperatures. For instance, the ED approach gives accurate results from T=0 up to T=250 K.[24] In turn Hirsch-Fye QMC is

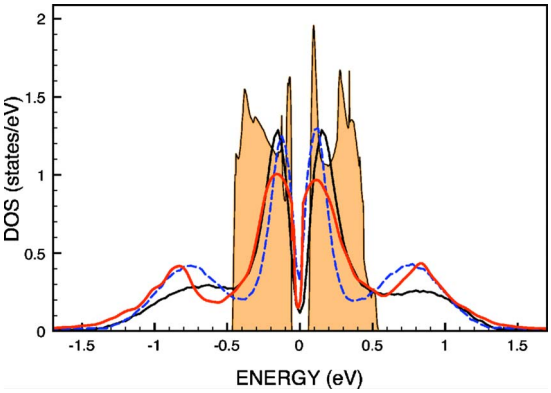

FIG. 7. (Color online) Spectral functions obtained from the DMFT calculations using QMC-HF (blue dashed line), CT-QMC (black solid line), and exact diagonalization (red solid line) techniques at $T=232$ K. Orange filled area corresponds to the LDA density of states.

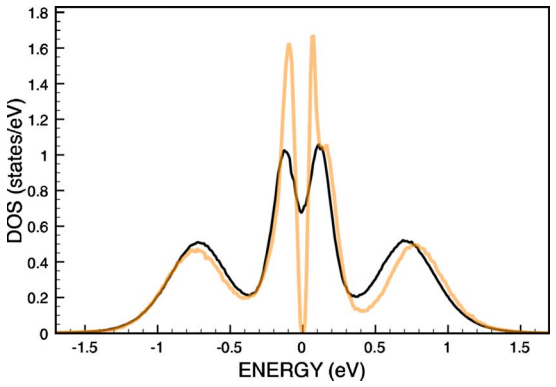

FIG. 8. (Color online) Densities of states obtained from the QMC-HF calculations at $T=386$ K (black line) and 96 K (orange line).

well suited for relatively high temperatures from 100 K up to 1000 K. The QMC methods require a maximum entropy method for analytical continuation of the resulting Green's function to real-energy axis.

The authors of Ref. 27 have shown that one should vary the value of the on-site Coulomb interaction in order to fit different experimental data. In our investigation the value of the on-site Coulomb interaction parameter U was fitted to obtain the best agreement with experimentally observed band narrowing $m^*=2$. We have chosen $U=1$ eV that is close to the value used in Ref. 14. This rather small value can be justified by an effective screening of d-d Coulomb interaction due to a strong Fe-ligand hybridization as it was demonstrated in constrain DFT calculation of the Coulomb interaction parameter U for LaOFeAs.[25]

The resulting paramagnetic densities of states calculated in DMFT at $T=232$ K are presented in Fig. 7. One can see that all the methods result in a pseudogapped state with a strongly renormalized density of states near the Fermi level. There are satellites at $\pm U/2$ which correspond to the lower and upper Hubbard bands.

The energy area around the Fermi level corresponds to quasiparticle states that are usually described as noninteracting bands renormalized by Coulomb correlations. The renormalization process can be understood by a low-frequency analysis of the dynamical mean-field equations.[21] The lattice Green's function is given by

$$G(\omega) = \sum_{\mathbf{k}} [\omega - \Sigma(\omega) - \epsilon(\mathbf{k})]^{-1}, \tag{1}$$

where Σ is a self-energy and $\epsilon(\mathbf{k})$ is a LDA spectrum. We expand the real part of the self-energy in the vicinity of the Fermi energy leaving only linear term

$$\mathrm{Re}\,\Sigma(\omega) \approx \mathrm{Re}\,\Sigma(0) + \omega \left.\frac{d\,\mathrm{Re}\,\Sigma(\omega)}{d\omega}\right|_{\omega=0}. \tag{2}$$

Then Green's function for specific wave vector $\mathbf{k}$ is

$$G_{\mathbf{k}}(\omega) \approx [\omega m^* - \epsilon(\mathbf{k})]^{-1}, \tag{3}$$

where m^* is the effective band mass-renormalization parameter

$$m^* \equiv 1 - \left.\frac{d\,\mathrm{Re}\,\Sigma(\omega)}{d\omega}\right|_{\omega=0}. \tag{4}$$

Equation (3) can be rewritten as

$$G_{\mathbf{k}}(\omega) \approx \frac{Z}{\omega - \tilde{\epsilon}(\mathbf{k})}, \tag{5}$$

where $Z \equiv 1/m^*$ is a quasiparticle weight and $\tilde{\epsilon}(\mathbf{k}) \equiv \epsilon(\mathbf{k})/m^*$ is the dispersion of the renormalized band. Therefore, the renormalization for quasiparticle states near the Fermi level due to the Coulomb correlations results in a band structure narrowing by a factor of m^* and a reduction in the corresponding spectral weight by a factor of Z with the rest of the spectral weight transferred to the upper and lower Hubbard bands at $\pm U/2$.

In our DMFT calculations the effective band mass-renormalization parameter $m^* \approx 2$ was found in good agreement with the results of the ARPES (Ref. 15) showing band narrowing by a factor of 2 in comparison with bands calculated in LDA.

Experimentally, FeSi demonstrates transition from narrow-gap semiconductor to bad metal with the increase in temperature.[5] We performed DMFT calculations at different temperatures and such an experimentally observed transition was successfully reproduced theoretically. The DMFT spectral functions calculated at different temperatures are presented in Fig. 8. The energy gap of about 50 meV at $T=96$ K agrees well with experimental results of resistivity measurements which indicate a charge gap of about 60 meV.[26] At $T=386$ K the gap area is almost completely filled by a spectral weight transfer from the sharp peaks near the gap resulting in the spectral function corresponding to a bad metal. The energy gap value obtained in the DMFT calculation is two times smaller than the corresponding value from the LDA band structure calculations (0.1 eV). That agrees very well with the effective band mass-renormalization parameter $m^* \approx 2$ Eq. (4) obtained in our DMFT calculations.

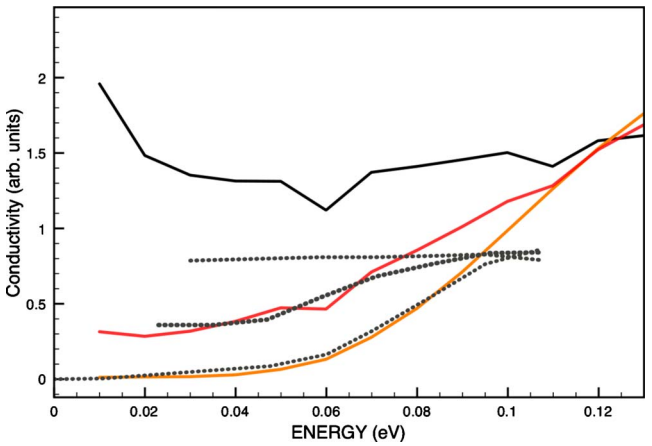

FIG. 9. (Color online) The convolution for FeSi model obtained from LDA+DMFT calculations in the framework of QMC-HF method at 386 K (black line), 232 K (red line), and 96 K (orange line). The grey dotted lines correspond to the experimentally observed optical conductivity at $T=20$ K, 150 and 250 K (taken from Ref. 4).

Optical spectroscopy experiments show gradual filling of the low-temperature energy gap with the temperature increase till complete gap disappearance above room temperature.[4] We estimated the optical conductivity by a spectral function convolution using the following expression:

$$\sigma(\omega,T)=\frac{1}{\omega}\int d\epsilon N(\epsilon)N(\epsilon+\omega)[1-f(\epsilon+\omega,T)], \qquad (6)$$

where $N(\epsilon)$ is a spectral function obtained from the DMFT calculations (Fig. 7) and $f(\epsilon,T)$ is the Fermi distribution function. The calculated convolution together with experimental data for temperature-dependent optical conductivity[4] is presented in Fig. 9.

At low temperatures a well-pronounced energy gap of about 0.05 eV can be observed in both experimental and theoretical curves. With the temperature increase optical conductivity increases at the energies below 0.05 eV and finally at $T=386$ K there is no any trace of the gap in the theoretical curve in good agreement with experimental data.

In the vicinity of the room-temperature FeSi displays an unusual crossover from a singlet semiconducting ground state with a narrow band gap to a metal with an enhanced spin susceptibility and Curie-Weiss temperature dependence.[1] All previous attempts to explain this behavior were based on the models assuming extremely narrow (<1000 K) peaks at the energy gap edges in DOS while LDA calculations gave band width nearly an order of magnitude larger than that value. Our DMFT calculations demonstrate that the correlated band insulator model with realistic DOS can reproduce anomalous temperature dependence of the magnetic susceptibility for FeSi. We computed $\chi(T)$ as a ratio

$$\chi(T)=\frac{M}{h}, \qquad (7)$$

where h is a small uniform external magnetic field and M is an induced magnetization of the system. In our DMFT calculations the external magnetic field acts only on spin motion and has no effect on orbital motion. The comparison of the experimental and calculated magnetic susceptibilities is presented in Fig. 10. We would like to stress that the stable DMFT solutions with a small magnetic moment were obtained at $T>200$ K. One can see that the calculated spin susceptibility reaches maximum at 600 K, which is in good agreement with the experimental temperature of 500 K. However, the calculated absolute values of the magnetic susceptibility at $T>300$ K disagree with experimentally observed $\chi(T)$. Such a disagreement was observed in the previous theoretical investigation.[27] Varying the Coulomb interaction U the authors of Refs. 27 and 28 were able to fit a theoretical curve to the experimental one.

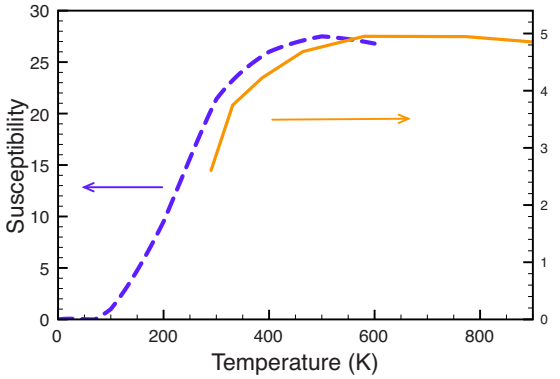

FIG. 10. (Color online) Spin susceptibility $\chi(T)$ (in μ_B^2/ eV) from the LDA+DMFT calculations with QMC-HF solver (orange solid line) and from experiment (Ref. 1) (blue dashed line).

In the present investigation the model DOS (Fig. 6) and Coulomb interaction parameter U value were used to successfully reproduce band narrowing observed in ARPES,[15] optical conductivity,[4] and temperature dependence of magnetic susceptibility.[1]

III. $Fe_{1-x}Co_xSi$

The correct theoretical description of magnetic properties of transition-metal monosilicides such as MnSi and $Fe_{1-x}Co_xSi$ alloys presents a longstanding problem of condensed matter physics. There has been a considerable amount of experimental and theoretical work on MnSi and $Fe_{1-x}Co_xSi$, regarding their structural, magnetic, and electronic properties. However, at the moment there is no satisfactory first-principles description of monosilicides magnetic properties. For instance, in case of MnSi it was found that the experimental value of the magnetic moment is about $0.4\mu_B$. Different first-principles calculations based on the density-functional theory gave much larger magnetic moment value of $1\mu_B$.[29,30]

$Fe_{1-x}Co_xSi$ alloys are magnetic for almost all of the intermediate concentration regimes,[6,31,32] while the end compounds FeSi and CoSi are nonmagnetic, the latter being a diamagnetic semimetal. $Fe_{1-x}Co_xSi$ system is also interesting for scientists due to the promising properties for spintronic device applications. For instance, in paper of Ref. 33 the authors have reported the discovery of a large anomalous

Hall effect for $Fe_{1-x}Co_xSi$. They have demonstrated that the large effect is most likely intrinsic—derived from the band structure effects rather than due to impurity scattering. They have proposed to consider the transition metal monosilicides as potential alternatives to the (GaMn)As and (GaMn)N which are the most popular materials for spintronics.

From theoretical side no calculation reported so far reproducing correctly both magnetic moment value and Curie temperature of $Fe_{1-x}Co_xSi$ system. To model the magnetic properties of $Fe_{1-x}Co_xSi$ alloys, the authors of paper of Ref. 34 used the full potential linearized augmented plane-wave method in combination with a virtual crystal approximation as well as with a supercell approach. The resulting magnetic moments agree well with experimental values only for $x < 0.25$. Having supposed an important role of ordering and segregation, they simulated several alloy configurations for concentrations $x \leq 0.5$. The weighted average magnetic moment that was calculated through Boltzmann distribution is in reasonable agreement with experimental value. However, there are no experimental results which support the segregation and ordering phenomena. Moreover, the results of neutron measurements[35] demonstrated a random distribution of transition metals in $Fe_{0.5}Co_{0.5}Si$.

To simulate randomly distributed $Fe_{1-x}Co_xSi$ alloys, the authors of Ref. 36 have used the combination of an exact muffin-tin orbitals method and a coherent potential approximation. They have found an extreme sensitivity of magnetic properties to the internal structure parameters and lattice constant. However, the calculated magnetic moments at concentrations $x > 0.3$ still disagreed with those experimentally observed.

In this paper we have investigated electronic structure and magnetic properties of $Fe_{1-x}Co_xSi$ alloys using static local spin density approximation (LSDA) and dynamical (DMFT) mean-field approaches. The virtual crystal approximation gives us the opportunity to investigate the electronic structure of $Fe_{1-x}Co_xSi$ system in whole range of concentrations. We found that LSDA results strongly overestimate magnetic moment values and extend magnetic phase diagram to much large values of Co concentration x comparing with experiment. An account of correlation effects within DMFT results in good agreement with experiment for magnetic moment values as well as the position of the magnetization $M(x)$ maximum. We concluded that $Fe_{1-x}Co_xSi$ is an itinerant electrons system which magnetic properties can be correctly described by the LDA+DMFT method.

A. Static mean-field results

The electronic structure of $Fe_{1-x}Co_xSi$ was calculated using the tight-binding linear muffin-tin orbital method in atomic sphere approximation with conventional LDA.[16] The Fe and Co atoms in $Fe_{1-x}Co_xSi$ alloy were treated by virtual atoms with the atomic number value averaged by the concentration x. The experimentally observed lattice constants[33] were used in the present band structure calculations. The calculated magnetic moment as a function of cobalt concentration is presented in Fig. 11 and densities of states for $x = 0.2$, 0.5, and 0.8 are presented in Fig. 12. One can see that

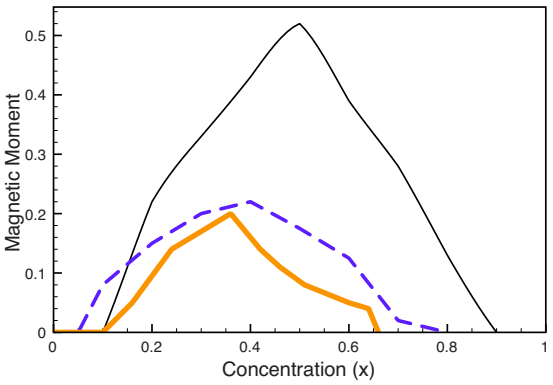

FIG. 11. (Color online) Concentration dependences of the magnetization per transition metal atom (in μ_B) obtained from the LDA+DMFT (orange bold line) and virtual crystal approximation (black thin line) in comparison with the neutron scattering experimental data (Ref. 6) (blue dashed line).

the calculated results start strongly deviate from experimental values of magnetic moments for Co concentration $x > 0.3$ with magnetization $M(x)$ maximum at $0.5\mu_B$ instead of experimental value of about $0.2\mu_B$ and giving stable magnetism for larger x values than it is observed experimentally. Our results agree well with those presented in Refs. 34 and 36.

A small magnetic moment value calls the question of the nature of magnetism in $Fe_{1-x}Co_xSi$: do we see itinerant electrons magnetism of the Stoner type or moments are local but their average value is suppressed due to quantum fluctuations and disorder effects? In order to investigate the localization degree of the magnetic moment in $Fe_{1-x}Co_xSi$ system we performed the supercell calculation to simulate a Co impurity in FeSi. The supercell was constructed in the FeSi lattice with all basis lattice vectors doubled and containing a total of 32 atoms of transition metal. The impurity Co atom was assumed to substitute one of Fe atom. The obtained magnetization spatial distribution in $Fe_{31}CoSi_{32}$ is presented in Fig. 13. One can see that the magnetic moment is not localized on the Co impurity. There is a magnetic cluster containing one cobalt atom and six nearest iron atoms. This is a result of a strong hybridization of $3d$ states cobalt and iron through $3s$ and $3p$ states of silicon.

The fact that the magnetic moment induced in FeSi by Co alloying is delocalized supports the itinerant magnetism picture. In this case the Stoner approach is expected to give a realistic description of $Fe_{1-x}Co_xSi$ magnetic properties. However, the results of this section and previous works show that direct Stoner theory application leads to a substantial overestimation of the magnetic moment value at intermediate concentrations (Fig. 11). This is a result of ignoring dynamical correlation effects that, as we will show below, result in a strong renormalization of states near the Fermi level and subsequent reduction in the magnetic moment value.

B. Dynamical mean-field results

In this section we investigate the influence of dynamical correlation effects on the magnetic properties of $Fe_{1-x}Co_xSi$.

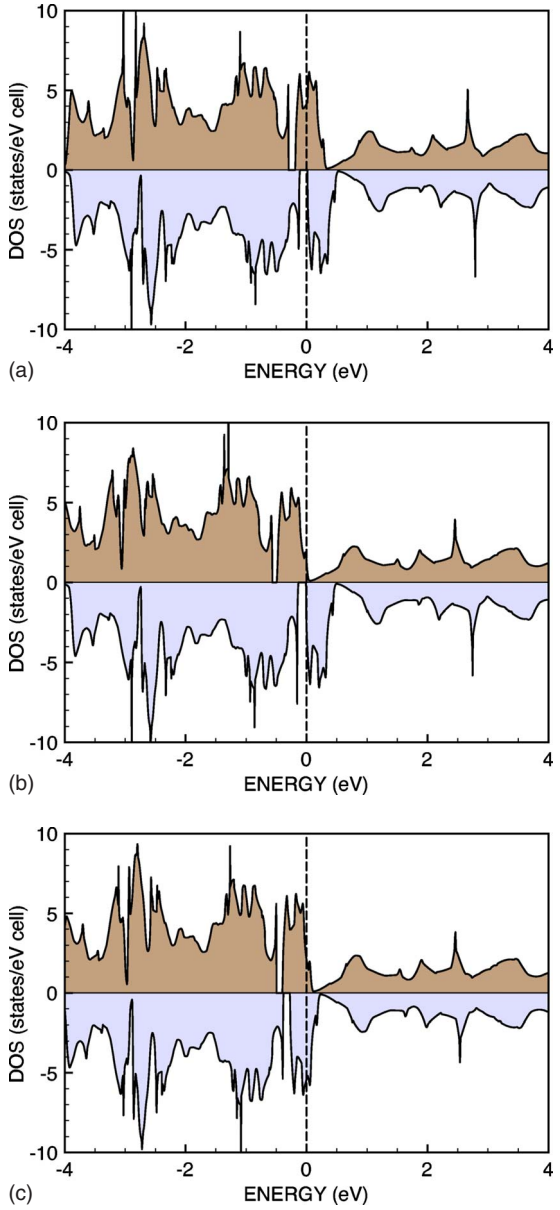

FIG. 12. (Color online) Densities of states for $x=0.2$, 0.5, and 0.8 obtained in the LSDA calculations based on virtual crystal approximation.

In our calculations we assume that Coulomb correlations treated by DMFT renormalize a paramagnetic density of states and then this new DOS is used as an input for Stoner theory calculations.

Let us first qualitatively discuss the origin of magnetism of the investigated alloys using the Stoner criterion

$$I_d N(E_F) > 1. \tag{8}$$

Assuming the Stoner parameter I_d value is equal to 1 eV the magnetic ground state is stable if the density of states at the Fermi level $N(E_F)$ is larger than 1 states/eV. With Co substituting Fe in FeSi number of electrons per formula unit increases and the Fermi level runs through the peak above the energy gap. Hence for $Fe_{1-x}Co_xSi$ the value of $N(E_F)$ is determined by the height of the peak. In DMFT the spectral

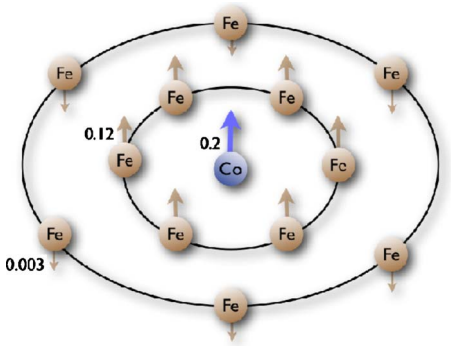

FIG. 13. (Color online) Schematic representation of a magnetic cluster simulated with the LSDA supercell calculations. Numbers are values of magnetic moments of ions (in μ_B) from different coordination spheres. The arrows denote directions of the magnetic moments in the ground state.

function depends on the temperature. Figure 14 gives DMFT densities of states obtained at $T=58$ K and $T=232$ K by using the exact diagonalization technique. One can see that the density of states value at the peak maximum is larger than 1 states/eV at $T=58$ K but becomes less than 1 at $T=232$ K. Then the Stoner criterion for magnetism Eq. (8) is satisfied for $T=58$ K but not for $T=232$ K. This result agrees with the experimental value of the Curie temperature $T_c=50$ K.

We are now in a position to perform the quantitative analysis of the magnetism. The DMFT calculations for $Fe_{1-x}Co_xSi$ were carried out for various concentrations x. The results for $x=0.36$ and $x=0.66$ are presented in Fig. 15. One can see that for $x=0.36$ the density of states at the Fermi level $N(E_F)>1$ and for $x=0.66$ $N(E_F)<1$. According to the Stoner criterion Eq. (8) that gives magnetic and nonmagnetic ground states for $x=0.36$ and $x=0.66$, correspondingly, in good agreement with experimental data (see Fig. 11).

We have used the obtained paramagnetic DMFT densities of states for different concentrations (Fig. 15) to solve the Stoner model. Self-consistent values for spin-up $n_\uparrow$ and spin-down $n_\downarrow$ numbers of electrons are given by equations for the total magnetic moment

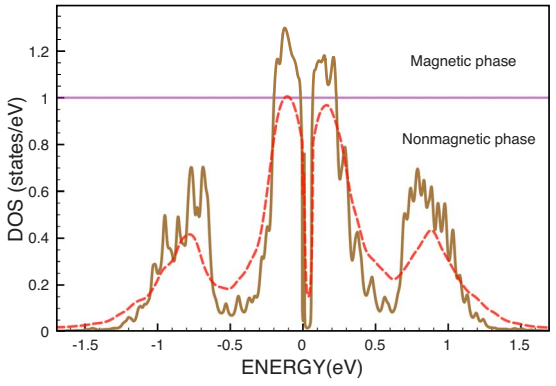

FIG. 14. (Color online) Densities of states for FeSi obtained by using exact diagonalization DMFT method at $T=232$ K (red dashed line) and $T=58$ K (brown solid line).

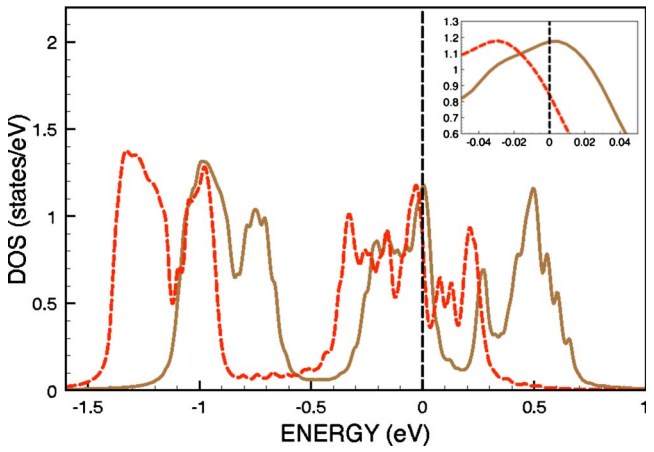

FIG. 15. (Color online) Densities of states of the doped FeSi model obtained by using the exact diagonalization DMFT method at $T=58$ K for $x=0.36$ (brown solid line) and $x=0.66$ (red dashed line). The densities of states near the Fermi level are presented in the inset. The black dashed line corresponds to the Fermi level.

$$M = \int_{-\infty}^{+\infty} [N(\epsilon + I_d n_\uparrow) - N(\epsilon + I_d n_\downarrow)] f(\epsilon, T) d\epsilon \qquad (9)$$

and the total number of electrons

$$N = \int_{-\infty}^{+\infty} [N(\epsilon + I_d n_\uparrow) + N(\epsilon + I_d n_\downarrow)] f(\epsilon, T) d\epsilon \qquad (10)$$

that are recalculated iteratively. Here $N(\epsilon)$ is a density of states obtained in the DMFT calculations and $f(\epsilon, T)$ is the Fermi distribution function. The Stoner parameter I_d was chosen to be 1 eV close to that used in previous theoretical estimations.[36]

The calculated concentration dependence of magnetization $M(x)$ is presented in Fig. 11. There is good agreement between experimental and theoretical values. The main effect of using $\rho(\epsilon)$ obtained in DMFT is a strong reduction in the resulting magnetic moment values compared to calculations using the unrenormalized LDA DOS. This reduction is due to the quasiparticle weight factor $Z \equiv 1/m^*$ appearing in the numerator for Green's function expression Eq. (5). Then the integral over quasiparticle band states near the Fermi level is decreased by a factor of Z comparing with unrenormalized LDA values. As $Z \approx 0.5$ in our DMFT calculations that results in corresponding decrease in $M(x)$ values by this factor.

IV. DISCUSSION

In this paper we have investigated electronic structure and magnetic properties of FeSi and $Fe_{1-x}Co_xSi$ systems using static and dynamical mean-field approaches. Our band structure analysis supports the correlated band insulator model for these materials in contrast to the Kondo insulator model. The results of the DMFT calculations revealed a strong renormalization of states near the Fermi level. The estimated band-mass renormalization $m^* \approx 2$ agrees well with that obtained in the recent ARPES experiments. Analyzing paramagnetic DMFT densities of states calculated at different temperatures and at different Co concentrations we demonstrated that itinerant magnetism picture is valid for $Fe_{1-x}Co_xSi$ alloys.

ACKNOWLEDGMENTS

The hospitality of the Institute of Theoretical Physics of Hamburg University (Grant No. SFB 668) and the Institute of Theoretical Physics of ETH-Zurich is gratefully acknowledged. We would like to thank T. M. Rice, M. Sigrist, A. Läuchli, Y. Yamashita, D. van der Marel, and I. Solovyev for helpful discussions, and Y. O. Kvashnin for his assistance with Wannier function analysis. This work is supported by the grant program of President of Russian Federation under Grant No. MK-1162.2009.2, by the scientific program "Development of scientific potential of universities" under Grant No. N 2.1.1/779, by the scientific program of the Russian Federal Agency of Science and Innovation under Grant No. N 02.740.11.0217, President of Russian Federation fund for support for scientific schools under Grants No. NSH 1941.2008.2, No. RFFI 07-02-00041, and No. RFFI-09-02-00431a, grants of the Ural Division of the Russian Academy of Sciences N7 and N28. The calculations were performed on the computer cluster of "University Center of Parallel Computing" of USTU-UPI.

[1] V. Jaccarino, G. K. Wertheim, J. H. Wernick, L. R. Walker, and S. Arajs, Phys. Rev. **160**, 476 (1967).
[2] H. Watanabe, H. Yamamoto, and K. Ito, J. Phys. Soc. Jpn. **18**, 995 (1963).
[3] K. Ishizaka, T. Kiss, T. Shimojima, T. Yokoya, T. Togashi, S. Watanabe, C. Q. Zhang, C. T. Chen, Y. Onose, Y. Tokura, and S. Shin, Phys. Rev. B **72**, 233202 (2005).
[4] Z. Schlesinger, Z. Fisk, Hai-Tao Zhang, M. B. Maple, J. F. DiTusa, and G. Aeppli, Phys. Rev. Lett. **71**, 1748 (1993).
[5] S. Paschen, E. Felder, M. A. Chernikov, L. Degiorgi, H. Schwer, H. R. Ott, D. P. Young, J. L. Sarrao, and Z. Fisk, Phys. Rev. B **56**, 12916 (1997).
[6] J. Beille, J. Voiron, and M. Roth, Solid State Commun. **47**, 399 (1983); K. Ishimoto, Y. Yamaguchi, S. Mitsuda, M. Ishida, and Y. Endoh, J. Magn. Magn. Mater. **54-57**, 1003 (1986).
[7] Y. Takahashi, J. Phys.: Condens. Matter **9**, 2593 (1997).
[8] D. Mandrus, J. L. Sarrao, A. Migliori, J. D. Thompson, and Z. Fisk, Phys. Rev. B **51**, 4763 (1995).
[9] C. Fu and S. Doniach, Phys. Rev. B **51**, 17439 (1995).
[10] M. Fath, J. Aarts, A. A. Menovsky, G. J. Nieuwenhuys, and J. A. Mydosh, Phys. Rev. B **58**, 15483 (1998).
[11] Z. Fisk, J. L. Sarrao, S. L. Cooper, P. Nyhus, G. S. Boebinger, A. Passner, and P. C. Canfield, Physica B (Amsterdam) **223-224**, 409 (1996).
[12] L. F. Mattheiss and D. R. Hamann, Phys. Rev. B **47**, 13114 (1993).

[13] T. E. Mason, G. Aeppli, A. P. Ramirez, K. N. Clausen, C. Broholm, N. Stücheli, E. Bucher, and T. T. M. Palstra, Phys. Rev. Lett. **69**, 490 (1992).
[14] J. Kuneš and V. I. Anisimov, Phys. Rev. B **78**, 033109 (2008).
[15] M. Klein, D. Zur, D. Menzel, J. Schoenes, K. Doll, J. Röder, and F. Reinert, Phys. Rev. Lett. **101**, 046406 (2008).
[16] O. K. Andersen, Phys. Rev. B **12**, 3060 (1975); O. K. Andersen and O. Jepsen, Phys. Rev. Lett. **53**, 2571 (1984).
[17] J. F. Janak, V. L. Moruzzi, and A. R. Williams, Phys. Rev. B **12**, 1257 (1975).
[18] V. I. Anisimov, S. Y. Ezhov, I. S. Elfimov, I. V. Solovyev, and T. M. Rice, Phys. Rev. Lett. **76**, 1735 (1996).
[19] G. H. Wannier, Phys. Rev. **52**, 191 (1937); N. Marzari and D. Vanderbilt, Phys. Rev. B **56**, 12847 (1997); W. Ku, H. Rosner, W. E. Pickett, and R. T. Scalettar, Phys. Rev. Lett. **89**, 167204 (2002); V. I. Anisimov, D. E. Kondakov, A. V. Kozhevnikov,
I. A. Nekrasov, Z. V. Pchelkina, J. W. Allen, S.-K. Mo, H.-D. Kim, P. Metcalf, S. Suga, A. Sekiyama, G. Keller, I. Leonov, X. Ren, and D. Vollhardt, Phys. Rev. B **71**, 125119 (2005).
[20] V. V. Mazurenko, S. L. Skornyakov, V. I. Anisimov, and F. Mila, Phys. Rev. B **78**, 195110 (2008).
[21] A. Georges, G. Kotliar, W. Krauth, and M. J. Rozenberg, Rev. Mod. Phys. **68**, 13 (1996).
[22] J. E. Hirsch and R. M. Fye, Phys. Rev. Lett. **56**, 2521 (1986).
[23] A. N. Rubtsov, V. V. Savkin, and A. I. Lichtenstein, Phys. Rev. B **72**, 035122 (2005).
[24] M. Capone, L. de' Medici, and A. Georges, Phys. Rev. B **76**, 245116 (2007).
[25] V. I. Anisimov, Dm. M. Korotin, M. A. Korotin, A. V. Kozhevnikov, J. Kuneš, A. O. Shorikov, S. L. Skornyakov, and S. V. Streltsov, J. Phys.: Condens. Matter **21**, 075602 (2009).
[26] A. Lacerda, H. Zhang, P. C. Canfield, M. F. Hundley, Z. Fisk, J. D. Thompson, C. L. Seaman, M. B. Maple, and G. Aeppli, Physica B **186-188**, 1043 (1993).
[27] K. Urasaki and T. Saso, Phys. Rev. B **58**, 15528 (1998).
[28] K. Urasaki and T. Saso, J. Phys. Soc. Jpn. **68**, 3477 (1999).
[29] T. Jeong and W. E. Pickett, Phys. Rev. B **70**, 075114 (2004).
[30] P. Lerch and T. Jarlborg, J. Magn. Magn. Mater. **131**, 321 (1994).
[31] J. Beille, J. Voiron, F. Towfiq, M. Roth, and Z. Y. Zhang, J. Phys. F: Met. Phys. **11**, 2153 (1981).
[32] N. Manyala, Y. Sidis, J. F. DiTusa, G. Aeppli, D. P. Young, and Z. Fisk, Nature (London) **404**, 581 (2000).
[33] N. Manyala, Y. Sidis, J. F. DiTusa, G. Aeppli, D. P. Young, and Z. Fisk, Nature Mater. **3**, 255 (2004).
[34] J. Guevara, V. Vildosola, J. Milano, and A. M. Llois, Phys. Rev. B **69**, 184422 (2004).
[35] F. Mezei, J. Schweizer, V. Jaccarino, and J. H. Wernick, Solid State Commun. **20**, 533 (1976).
[36] M. P. J. Punkkinen, K. Kokko, M. Ropo, I. J. Vayrynen, L. Vitos, B. Johansson, and J. Kollar, Phys. Rev. B **73**, 024426 (2006).